Organic & Biomolecular Chemistry

PAPER

View Article Online
View Journal | View Issue

Check for updates

Cite this: *Org. Biomol. Chem.*, 2017, **15**, 8641

Computational characterization of the mechanism for the light-driven catalytic trichloromethylation of acylpyridines†

Victor M. Fernandez-Alvarez[a] and Feliu Maseras *[a,b]

Received 24th July 2017,
Accepted 22nd September 2017

DOI: 10.1039/c7ob01826f

rsc.li/obc

The computational characterization of the mechanism for complex reactions involving the photoactivation of transition metal compounds remains a challenge for theoretical chemistry. In this work we show how the application of DFT and ONIOM(DFT:MM) methods can characterize the photoinduced iridium-catalyzed enantioselective trichloromethylation of 2-acylpyridines that was recently reported by Meggers and co-workers. This is a complex process, as it involves two linked catalytic cycles and yields the product with high enantioselectivity. Calculations succeed in reproducing all available experimental data, including the sign and value of the enantiomeric excess. The detailed mechanistic picture that is obtained leads to the identification of the origin of selectivity as the steric repulsion between an attacking trichloromethyl radical and the ligands at iridium in the path leads to the minor enantiomer.

Published on 22 shtator 2017. Downloaded by Fail Open on 7.5.2025 10:15:08 e paradites.

Trichloromethyl groups are known to contribute to the pharmacological properties of several natural products.[1–3] Significant efforts have been put into strategies for the stereoselective insertion of this group into organic molecules involving both stoichiometric[4,5] and catalytic approaches (the latter mainly with Ru[6,7] and Ti[8,9] catalysts). However, effective approaches for the enantioselective addition of this unit have so far been limited. Many of the strategies used involve redox-mediated radical addition, thus presenting an opportunity for a photocatalytic approach. Photoredox catalysis enables the generation of highly reactive radicals under mild conditions,[10] but the low activation energy of follow up reactions constitutes a challenge for controlling asymmetric processes. To overcome this obstacle, strategies have been developed in which two catalysts work in tandem for a single reaction.[11] In this approach, photosensitizers capable of inducing electron transfer are combined with asymmetric co-catalysts which are mostly chiral organocatalysts that act as both the chiral centers and the Lewis acid sites.[12–15] Yet, a more desirable approach is to employ a single catalyst which can act both as the photosensitizer and the asymmetric catalyst.

Earlier studies towards this goal involved high energy UV light in combination with Lewis acid and hydrogen bonding interactions to perform enantioselective catalysis.[16–18] Most of the current visible-light photosensitizers, however, are cyclometallated Ir or Ru transition metal complexes,[19,20] and it is widely known that chiral metal complexes can catalyze asymmetric transformations.[21] With this in mind, Meggers and co-workers[22] developed a system capable of photoinducing a single electron transfer to enable the enantioselective trichloromethylation of 2-acyl imidazoles and 2-acylpyridines (Fig. 1). Here, a chiral Λ-iridium complex acts as both the photosensitizer and the asymmetric catalyst.[23] Complex (**I**) is an octahedral iridium centre with two bidentate achiral ligands in a left-handed propeller-type arrangement, which is the origin of chirality in the system.[24]

Computational chemistry is an established and valuable tool for the mechanistic study of processes in asymmetric catalysis,[25–29] and is making inroads in the description of

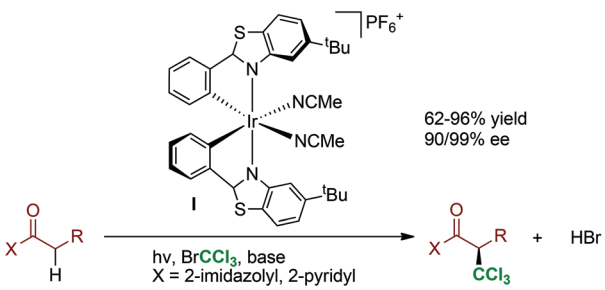

Fig. 1 General reaction scheme of the trichloromethylation.

[a]*Institute of Chemical Research of Catalonia, The Barcelona Institute for Science and Technology, Av. Paisos Catalans, 16, Tarragona 43007, Catalonia, Spain. E-mail: fmaseras@iciq.es; Fax: +34 977 920 231; Tel: +34 977 920 202*
[b]*Departament de Química, Universitat Autònoma de Barcelona, 08193 Bellaterra, Catalonia, Spain*

†Electronic supplementary information (ESI) available: Excitation computed by TD-DFT, components of SET calculations and Cartesian coordinates and total energies of all computed species. See DOI: 10.1039/C7OB01826F

Published on 22 shtator 2017. Downloaded by Fail Open on 7.5.2025 10:15:08 e paradites.

photoactivated processes.[30–32] Therefore, we set out to study this reaction using DFT methods to elucidate the factors that affect enantioselectivity and attempt to predict a system which might produce better enantioselectivity under experimental conditions. We chose 1-(pyridin-2-yl)propan-1-one (**1**) as the substrate, which forms the trichloromethyl-substituted pyridine derivative (**3**) with 67% yield and 95% enantiomeric excess.

Computational details

DFT and DFT/MM calculations were carried out using the Gaussian 09 software.[33] Two different sets of calculations were carried out. First we studied the full catalytic cycle on a model system with pure DFT calculations at the ωB97X-D level.[34] The basis set was LANL2DZ plus an additional f shell (exponent = 0.938) for Ir, and 6-31+G(d) for all other atoms.[35–37] The validity of the basis set was confirmed through single point calculations on key transition states with LANL2TZ(f) for Ir and 6-311+G(d) for other atoms. All geometry optimizations for this first set of calculations were carried out in methanol solution *via* the SMD model.[38] A second set of calculations was carried out at the ONIOM(ωB97X-D:UFF) level on the key transition states for a variety of systems. The QM/MM partition consisted in placing *tert*-butyl groups (or the groups replacing them) in the photocatalyst in the MM region. The description for the QM part was the same as described above. DFT/MM geometry optimizations were carried out under vacuum. Free energy corrections were taken from this ONIOM calculation, and the potential energies were refined by full QM single point calculations in solution. All reported energies are Gibbs energies at 298 K under 1 atm. Low frequencies were converted to 100 cm^{-1} following recent suggestions in the bibliography.[39,40] A data set collection of the computational results obtained with Gaussian 09 is available in the ioChem-BD repository[41] and can be accessed *via* http://doi:10.19061/iochembd-1-48.

Single electron transfer (SET) barriers were estimated using Marcus theory,[42,43] where the energy barrier is defined by using eqn (1). ΔG is the free energy difference between reactants and products, and λ is the reorganization energy of all nuclei involved in the SET, including solvent molecules. The reorganization energy was computed separately for each component (nuclear reorganization (λ_N) and solvent reorganization (λ_S)):

$$\Delta G^{\ddagger} = \frac{(\Delta G + \lambda)^2}{4\lambda} \quad (1)$$

λ_N was obtained by calculating the energy cost of changing the charge distribution between fragments while maintaining the same geometry. If the reaction is between an anionic donor D^- and a neutral acceptor A, both of them start at their optimal geometries $D_{D^-}{}^-$ and A_A, but increase their energies after the electron transfer to a D_{D^-} plus $A_A{}^-$ arrangement. This is numerically computed in eqn (2). This component of the total λ is by far the smallest one,[42] as can be seen in the values reported in the ESI.†

$$\lambda_N = D_{D^-} + A_A{}^- - D_{D^-}{}^- - A_A \quad (2)$$

The solvent reorganization energy (λ_S) was computed using the continuum solvent model. We indicate the solvation environment as a superscript, and the resulting eqn (3) is analogous to that above. This method to obtain the solvent reorganization energy has been used successfully to reproduce experimental results.[44,45]

$$\lambda_S = D^{[D^-]} + A^{-[A]} - D^{-[D^-]} - A^{[A]} \quad (3)$$

Results and discussion

Full catalytic cycle

Our first set of calculations used a model system for the photocatalyst, in which *tert*-butyl groups were replaced by methyl. We started by checking the mechanism proposed by Meggers and co-workers, which was found to be correct. Like many mechanisms in photoredox catalysis, it consists of two linked cycles, as shown in Fig. 2. The two cycles are connected through the transfer of the CCl_3 radical generated in the "light" cycle to the "dark" one and through a single electron transfer labeled as SET2. The peculiarity of this system is that the photosensitizer is one of the species in the "dark" catalytic cycle. Thus, two units of the intermediate **5** need to be generated.

The computed free energy profile is presented in Fig. 3. There is a certain scrambling in the sequence of the labels because some species appear in the two interlinked cycles. For the sake of simplicity, the initial catalyst **2**, used as the origin of relative energies, is considered in a tetracoordinate form, without the two acetonitrile ligands present in the precursor. Hexa- or pentacoordinate forms may indeed be more stable, but their explicit consideration would complicate the cycle without adding much chemical insight. Coordination of substrate **1** stabilizes the free catalyst (by 8.9 kcal mol^{-1}). Proton abstraction by lutidine from **4** results in complex **5**, in a step which is endergonic by 11.2 kcal mol^{-1}. Deprotonation through $\mathbf{TS_{PA}}$ has the highest thermal barrier in the catalytic cycle at 22.1 kcal mol^{-1}, a value which is nevertheless still affordable at room temperature. The complex **5** then absorbs a photon. A TD-DFT calculation predicts for this complex the existence of a strong metal–ligand charge transfer (MLCT) band at 387 nm with an oscillator strength of 0.1482. The excited state then relaxes to a phosphorescent triplet complex **8** at 58.1 kcal mol^{-1} above the reactants. This triplet complex can transfer one electron (**SET1**) to CCl_3Br with a low barrier (computed through Marcus theory) of 5.1 kcal mol^{-1}. This SET process results in three fragments: the cationic complex **9**, the CCl_3 radical, and a bromide anion. These three fragments have a total relative energy 17.3 kcal mol^{-1} above the initial reactants. The bromide anion is lost in the reaction media, and the two other fragments continue the reaction. The CCl_3 radical enters the "dark" cycle, reacting with another unit of the complex **5** to make a new C–C bond, in a low-barrier and highly exergonic step. This is the stereoselectivity-determining step, with two parallel paths that will be analyzed in detail in a later section. We mention here

 This journal is © The Royal Society of Chemistry 2017

Published on 22 shtator 2017. Downloaded by Fail Open on 7.5.2025 10:15:08 e paradites.

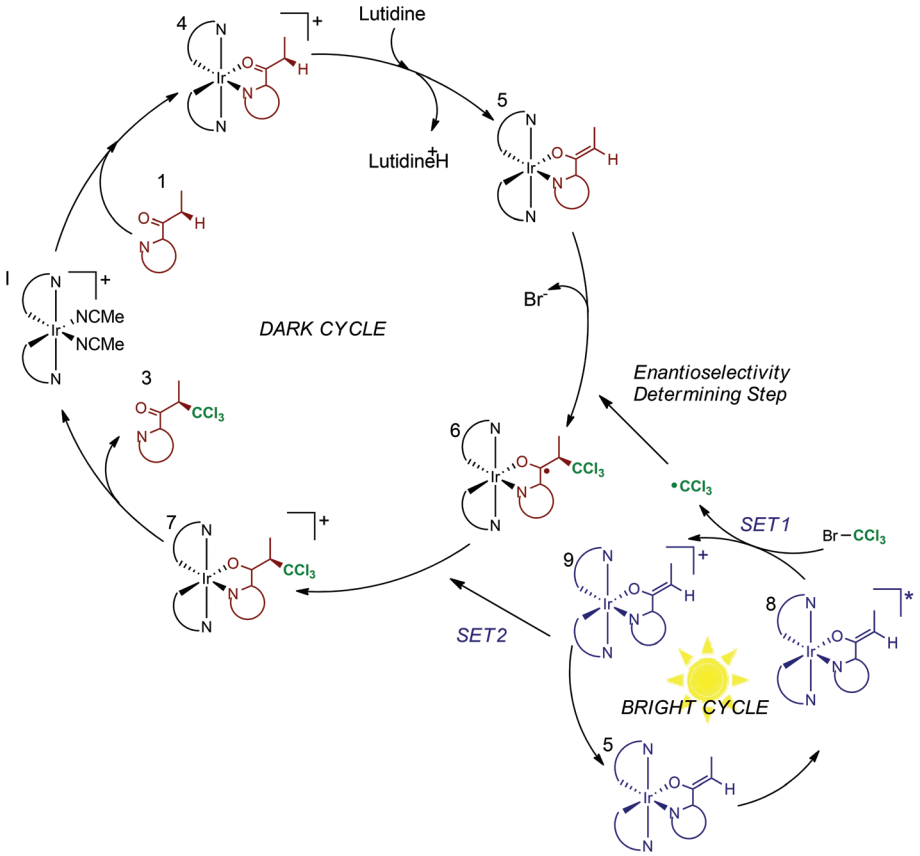

Fig. 2 Reaction mechanism for the trichloromethylation process.

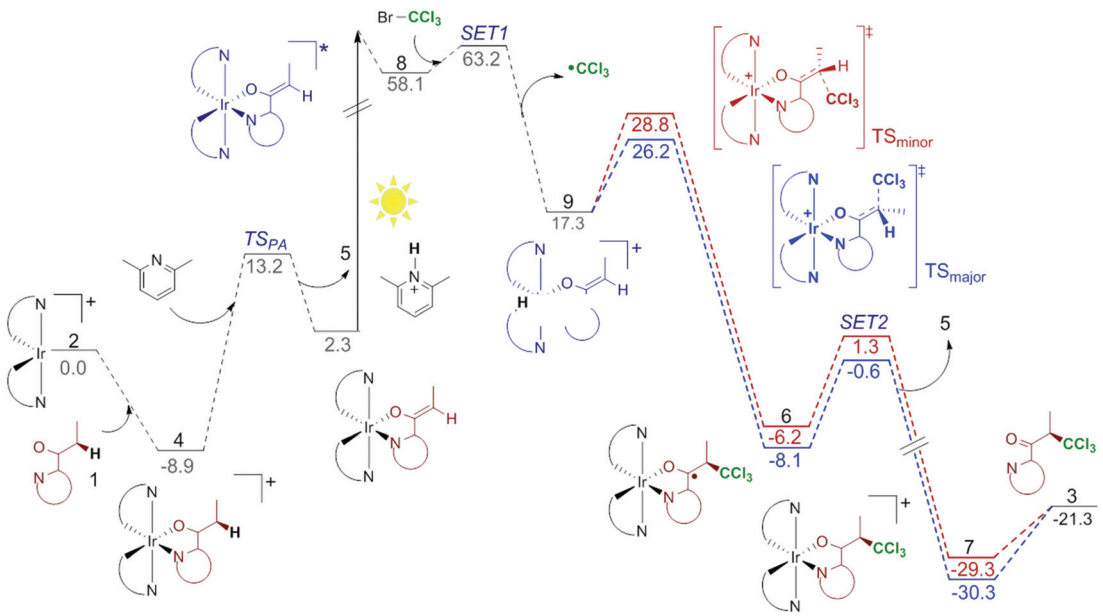

Fig. 3 Free energy profile of the trichloromethylation mechanism with the model catalyst. Energies in kcal mol^{-1}.

that we used the relative free energies of these critical transition states to benchmark the validity of our computational method. The calculation with a larger basis set (see computational details) modified the difference between them by only 0.2 kcal mol^{-1} (from 2.6 to 2.8 kcal mol^{-1}), thus confirming the validity of our method.

Published on 22 shtator 2017. Downloaded by Fail Open on 7.5.2025 10:15:08 e paradites.

The C–C bond formation generates the intermediate **6**. In the path depicted in Fig. 3, this intermediate transfers one electron back (**SET2**) to cation **9** in the "light" cycle to restore the photosensitizer **5**. The removal of one electron from **6** results in the cationic trichloromethylated complex **7**. Product **3** can easily dissociate from **7**, which results in the regeneration of the catalyst. **SET2** has an energy barrier of 7.4 kcal mol^{-1}, and the dissociation of **3** has an energy cost of 9.0 kcal mol^{-1}. Thus, the process is downhill and with low barriers after the formation of the C–C bond.

Propagation *vs.* termination

In addition to the cycle described above, the authors proposed that the direct electron transfer from **6** to CCl_3Br can also take place. We carried out calculations on this possibility and the results are summarized in Fig. 4.

The intermediate **6** can transfer an electron to the transient intermediate **9** through **SET2**, as indicated above, in what constitutes a termination pathway, but it can also transfer one electron to CCl_3Br through **SET3**, in a propagation pathway. In this propagation pathway, no extra photons are involved. The energy barrier of **SET3** is 9.5 kcal mol^{-1} (9.4 for the minor product), which is higher than that of **SET2** (Fig. 4). The raw numbers in Fig. 4 would suggest that the termination pathway through **SET2** to dominate. However, as we have shown in a previous study,[30] the competition between these termination and propagation pathways is severely affected by the concentration of the species involved. In this case, **9** is a transient species formed by light absorption, thus in much lower concentration than CCl_3Br, which is a reactant. Therefore, initially propagation is more competitive than termination, which may account for the quantum yield of 5 observed experimentally.

Location of photoexcitation in the catalytic cycle

In the mechanism analyzed above, the photoinduced electron transfer step takes place after the light-driven generation of the triplet complex **8**, upon deprotonation by lutidine. There are however other species in the media which are potentially photoactive. We study in this subsection the light absorption properties of all species that precede the formation of **5** to determine whether there is any other plausible photosensitizer which could give rise to a productive process. Fig. 5 shows the

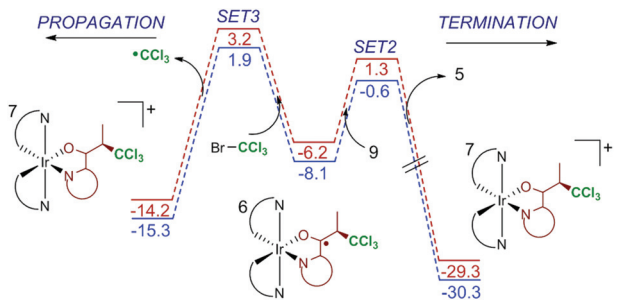

Fig. 4 Free energy profile showing the propagation/termination competition. Energies in kcal mol^{-1}.

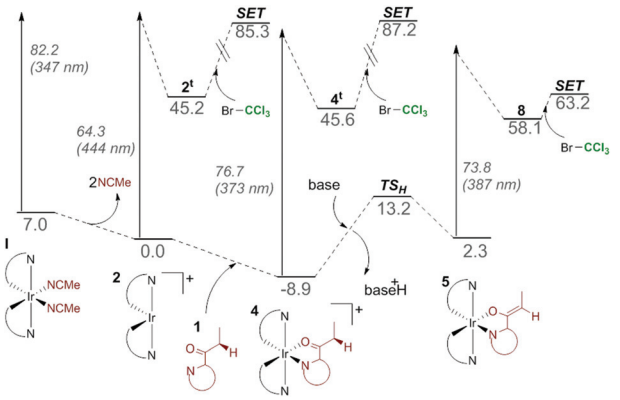

Fig. 5 Light absorption and electron transfer for different intermediates. Free energies in kcal mol^{-1}.

absorption energies and SET energy barriers for all intermediates up to **5**. The catalyst precursor **I** shows one significant metal–ligand charge transfer (MLCT) absorption band at 347 nm (oscillator strength f = 0.2912). This strong band is in agreement with the maximum absorption observed for the catalyst experimentally.[46] However, precursor **I** has to be discarded as a photosensitizer because the barrierless dissociation of the acetonitrile ligands leads to the formation of the lower energy complex **2**, indicating that the catalyst is entirely in the dissociated form.

Complex **2** is also able to absorb light, with an MLCT band at 444 nm (f = 0.0596). The corresponding triplet complex **2**^{t} relaxes to 45.2 kcal mol^{-1}. This complex is however unable to transfer an electron to CCl_3Br as the barrier for SET is prohibitively high (40.1 kcal mol^{-1}). Photoinduced electron transfer from **4** shows a similar pattern. The incorporation of a third bidentate electron-delocalizing ligand causes the appearance of a stronger MLCT band at 373 nm (f = 0.1704). However, SET to form the CCl_3 radical has a barrier of 41.6 kcal mol^{-1}, indicating that this complex is not the photosensitizer either.

Finally, complex **5** has a fully delocalized ligand system, which shifts the MLCT band to 387 nm (f = 0.1482). While higher in energy than the other complexes, **5** can act as the photosensitizer as the triplet state form **8** shows a low SET barrier (5.1 kcal mol^{-1}) towards the formation of the CCl_3 radical. Thus, our calculations confirm that the photosensitizer is indeed complex **5**.

Origin of enantioselectivity

We will discuss now the critical step where the C–C bond is formed and the stereoselectivity of the reaction is decided. The two transition states reported in Fig. 4 present low free energy barriers of 8.9 and 11.5 kcal mol^{-1}. The lowest energy transition state indeed leads to the experimentally reported major product. The predicted enantiomeric excess (ee) for this model system is 96%.

One could argue that our modeling of the ligand may affect enantioselectivity, and because of this we repeated the calculations with the real system, with full consideration of the *tert*-

 This journal is © The Royal Society of Chemistry 2017

Published on 22 shtator 2017. Downloaded by Fail Open on 7.5.2025 10:15:08 e paradites.

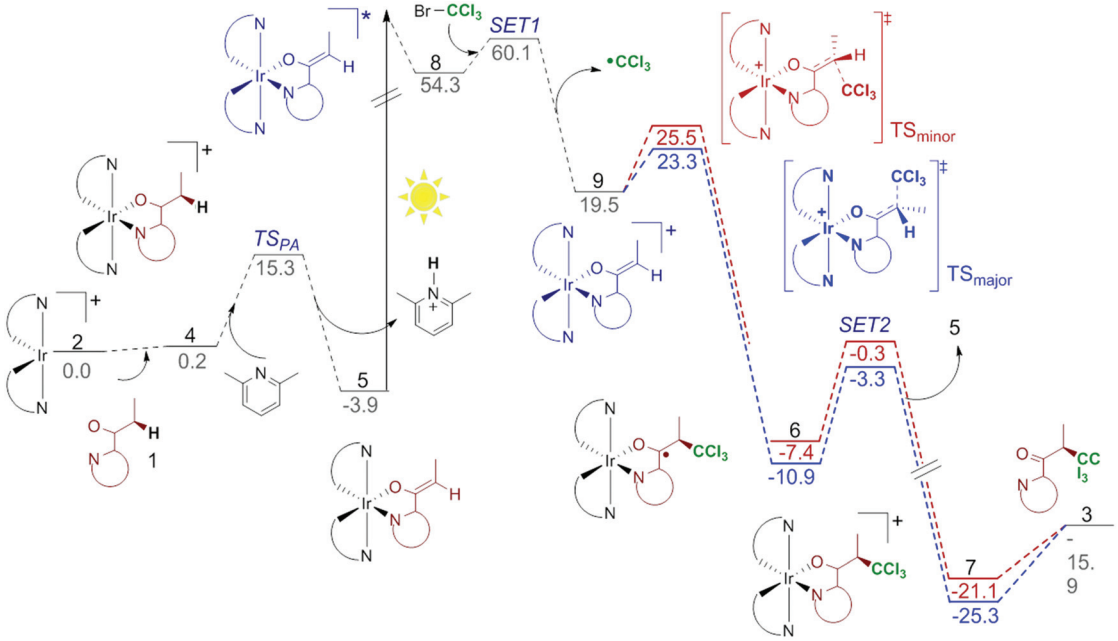

Fig. 6 Free energy profile of the trichloromethylation mechanism with the real catalyst. Energies in kcal mol^{-1}.

butyl substituents. Fig. 6 shows the resulting free energy profile. The calculated ee for the real system is 99%, which is still in good agreement with the experimental value of 95%. The calculated ee represents indeed an error in the free energy discrimination of only 0.7 kcal mol^{-1}. There are some minor differences between the two free energy profiles which are worth mentioning. The coordination of the reactant in the intermediate **4** is weaker in the real system, as the more constrained system is more reluctant to take an extra chelating ligand. The steric compression also favors neutral complexes with respect to cationic ones, as the sp^3 centers in **4** and **6** require more space than the sp^2 carbons in complexes like **5**. This has the interesting side effect of significantly lowering the barrier for deprotonation through $\mathbf{TS}_{PA}$, which is only 15.3 kcal mol^{-1} for the real system.

The structures obtained for the two competing transition states in the real system are presented in Fig. 7. An inspection of the geometries points to a steric origin for the enantioselectivity. The ligands present an octahedral arrangement around iridium. The chelating substrate which is essentially planar occupies two coordination sites in the equatorial plane in the orientation of the drawing. The CCl_3 radical will approach the carbon center in a direction approximately perpendicular to the plane. When it approaches the plane from above, in the drawing presentation, it will lead the major product. The attack from below will lead to the minor product. The approach of the CCl_3 radical is mostly unhindered in TS_{major}, as it does not get close to the substituents in the axial ligand. Things are different for TS_{minor}. The CCl_3 radical gets close to the "arm" of the axial ligand, and has to move away from the ideal perpendicular direction in order to avoid it. The particular nature of the ligands, resulting in these bulky

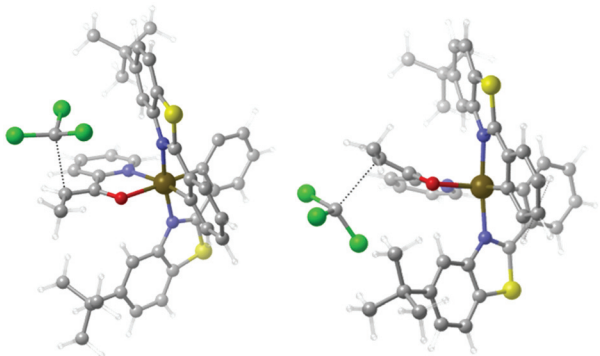

Fig. 7 Optimized geometries of the transition states leading to major (left) and minor (right) products.

groups in perpendicular planes, is of course at the origin of this stereoselectivity. It must be also mentioned that the problem is much simplified by the symmetry of the catalyst, which has only one possible conformation, significantly reducing the degrees of freedom in the mechanism.

Behavior of alternative systems

An experimental enantiomeric excess of 91% is very good, but still improvable. We decided to carry out computational experiments evaluating the selectivity associated with the hypothetical variations of the experimental catalyst. We studied the effect on the predicted enantioselectivity of the R substituent and the L linker in the ligand. These positions are occupied by *tert*-butyl and a sulfur atom in the experimental system (see Fig. 1). We calculated TS_{major} and TS_{minor} for the catalysts reported in Table 1. The experimental system corresponds to

Published on 22 shtator 2017. Downloaded by Fail Open on 7.5.2025 10:15:08 e paradites.

Table 1 Calculated ee for different catalysts

Catalyst	Substituent R	Linker L	Computed ee (%)
a	-H	S	91
b	-Methyl	S	96
c	-*tert*-Butyl	S	99
d	-Adamantyl	S	97
e	-*tert*-Butyl	HC═CH	33

complex (**c**) in the table. This is the only case where an experimental value for ee (95%) is available. We tried two systems with smaller R substituents: hydrogen (**a**) and methyl (**b**), and one with bulkier adamantyl groups (**d**). In addition, we calculated a catalyst in which the sulfur was replaced by HC═CH to increase the hindering effect of the ligand while maintaining aromaticity (**e**).

The resulting values for ee are collected in Table 1. We were to a certain extent surprised to find out that even the smallest substituent, hydrogen in system **a**, produced a respectable ee value of 91%. It is obvious that the presence of the ligand in this plane is sufficient to induce enantioselectivity (see Fig. 6). The values of ee for systems **b**, **c** and **d** are very similar, in the limits of accuracy of our computational method. We can in any case make a brief qualitative discussion on their differences. The increase in the substituent size of methyl (catalyst **b**) and *tert*-butyl (catalyst **c**) leads to predictable increases in computed selectivity to 96% and 99%, respectively. The approach of the CCl_3 radical in TS_{minor} is more hindered by bulkier ligands, as expected. However, the increase from *tert*-butyl to adamantyl (catalyst **d**) leads to a slight decrease, 99% to 97%.

Catalyst **e** has a significantly different behavior. The enantiomeric excess virtually disappears for this system (33%). The introduction of a HC═CH group places a 6-member ring in the ligand and pushes the ligand substituents towards the substrate. It increases clearly steric repulsion, but reduces enantioselectivity. The results indicate conclusively that the relation between steric repulsion and enantiomeric excess is not linear. When there is too much steric repulsion the structure of the octahedral complex is disrupted, and the approach of the CCl_3 radical in TS_{major} is also disfavored, thus diminishing selectivity.

Steric repulsion is thus the key to the selectivity of the process, but this repulsion reaches an optimal value for system **c**, that is reported experimentally. The introduction of additional steric effects distorts the system and reduces enantioselectivity.

Conclusion

We carried out calculations on the reaction mechanism of the trichloromethylation of 2-acylpyridines, and correctly reproduced the experimentally reported enantioselectivity, as well as other experimental observations. This adds strong support to the experimentally proposed existence of two linked catalytic cycles: a "dark" cycle, where the substrate is activated and the C–C bond is asymmetrically formed; and a "light" cycle, where the photosensitizer absorbs light and generates a CCl_3 radical from CCl_3Br by outer-sphere electron transfer. Our calculations also support the identification of the photosensitizer as the complex resulting from the deprotonation of the coordinated substrate.

The sign of enantioselectivity was correctly reproduced and a reasonable approach to the experimental value of ee was obtained: 99% *vs.* 95%. The origin of selectivity was identified as the steric hindrance in the approach of the CCl_3 radical to the complex, which in ideal cases only affects the formation of the minor product. The detailed picture provided by the calculations allowed us to evaluate the behavior of hypothetical catalysts with increased steric repulsion and led us to find that they also obstruct the path to the major product, thus reducing selectivity. The characterization of the reaction mechanism for such a complex system is a very promising result for the future role of theoretical chemistry in the characterization of photocatalytic and photoactivated processes. Calculation can access a mechanistic detail difficult to achieve from experiment, and hence be an important support for the further optimization of these increasingly relevant reactions.

Conflicts of interest

There are no conflicts of interest to declare.

Acknowledgements

The authors acknowledge financial support from the CERCA Programme (Generalitat de Catalunya) and MINECO (project CTQ2014-57661-R and Severo Ochoa Excellence Accreditation 2014-2018 SEV-2013-0319). V. F. is grateful to MINECO for an FPI fellowship (ref BES-2012-057655).

References

1 J. Orjala and W. H. Gerwick, *J. Nat. Prod.*, 1996, **59**, 427–430.
2 M. D. Unson, C. B. Rose, D. J. Faulkner, L. S. Brinen, J. R. Steiner and J. Clardy, *J. Org. Chem.*, 1993, **58**, 6336–6343.
3 W. Hofheinz and W. E. Oberhänsli, *Helv. Chim. Acta*, 1977, **60**, 660–669.
4 G. Helmchen and G. Wegner, *Tetrahedron Lett.*, 1985, **26**, 6047–6050.
5 S. E. Brantley and T. F. Molinski, *Org. Lett.*, 1999, **1**, 2165–2167.
6 S. Beaumont, E. A. Ilardi, L. R. Monroe and A. Zakarian, *J. Am. Chem. Soc.*, 2010, **132**, 1482–1483.
7 Z. Gu and A. Zakarian, *Angew. Chem., Int. Ed.*, 2010, **49**, 9702–9705.
8 Z. Gu, A. T. Herrmann and A. Zakarian, *Angew. Chem., Int. Ed.*, 2011, **50**, 7136–7139.

 This journal is © The Royal Society of Chemistry 2017

Published on 22 shtator 2017. Downloaded by Fail Open on 7.5.2025 10:15:08 e paradites.

9 T. Amatov and U. Jahn, *Angew. Chem., Int. Ed.*, 2011, **50**, 4542–4544.
10 M. Schmittel and A. Burghart, *Angew. Chem., Int. Ed. Engl.*, 1997, **36**, 2550–2589.
11 M. N. Hopkinson, B. Sahoo, J.-L. Li and F. Glorius, *Chem. – Eur. J.*, 2014, **20**, 3874–3886.
12 D. A. Nicewicz and D. W. C. MacMillan, *Science*, 2008, **322**, 77–80.
13 M. Neumann, S. Füldner, B. König and K. Zeitler, *Angew. Chem., Int. Ed.*, 2011, **50**, 951–954.
14 D. A. DiRocco and T. Rovis, *J. Am. Chem. Soc.*, 2012, **134**, 8094–8097.
15 J. Du, K. L. Skubi, D. M. Schultz and T. P. Yoon, *Science*, 2014, **344**, 392–396.
16 A. Bauer, F. Westkamper, S. Grimme and T. Bach, *Nature*, 2005, **436**, 1139–1140.
17 C. Müller, A. Bauer and T. Bach, *Angew. Chem., Int. Ed.*, 2009, **48**, 6640–6642.
18 R. Brimioulle and T. Bach, *Science*, 2013, **342**, 840–843.
19 K. Zeitler, *Angew. Chem., Int. Ed.*, 2009, **48**, 9785–9789.
20 C. K. Prier, D. A. Rankic and D. W. C. MacMillan, *Chem. Rev.*, 2013, **113**, 5322–5363.
21 P. Walsh and M. Kozlowski, *Fundamentals of Asymmetric Catalysis*, University Science Books, 2009.
22 H. Huo, C. Wang, K. Harms and E. Meggers, *J. Am. Chem. Soc.*, 2015, **137**, 9551–9554.
23 H. Huo, C. Fu, K. Harms and E. Meggers, *J. Am. Chem. Soc.*, 2014, **136**, 2990–2993.
24 E. B. Bauer, *Chem. Soc. Rev.*, 2012, **41**, 3153–3167.
25 D. M. Walden, O. M. Ogba, R. C. Johnston and P. H.-Y. Cheong, *Acc. Chem. Res.*, 2016, **49**, 1279–1291.
26 Q. Peng and R. S. Paton, *Acc. Chem. Res.*, 2016, **49**, 1042–1051.
27 C. Liu, M. Besora and F. Maseras, *Chem. – Asian J.*, 2016, **11**, 411–416.
28 J. Jover and F. Maseras, *Struct. Bonding*, 2016, **167**, 59–79.
29 J. Escorihuela, M. I. Burguete, G. Ujaque, A. Lledós and S. V. Luis, *Org. Biomol. Chem.*, 2016, **14**, 11125–11136.
30 V. M. Fernández-Alvarez, M. Nappi, P. Melchiorre and F. Maseras, *Org. Lett.*, 2015, **17**, 2676–2679.
31 L.-H. Liu, D. Wu, S.-H. Xia and G. Cui, *J. Comput. Chem.*, 2016, **37**, 2212–2219.
32 L. Dell'Amico, V. M. Fernandez-Alvarez, F. Maseras and P. Melchiorre, *Angew. Chem., Int. Ed.*, 2017, **56**, 3304–3308.
33 M. J. Frisch, G. W. Trucks, H. B. Schlegel, G. E. Scuseria, M. A. Robb, J. R. Cheeseman, G. Scalmani, V. Barone, B. Mennucci, G. A. Petersson, H. Nakatsuji, M. Caricato, X. Li, H. P. Hratchian, A. F. Izmaylov, J. Bloino, G. Zheng, J. L. Sonnenberg, M. Hada, M. Ehara, K. Toyota, R. Fukuda, J. Hasegawa, M. Ishida, T. Nakajima, Y. Honda, O. Kitao, H. Nakai, T. Vreven, J. A. Montgomery, J. E. Peralta, F. Ogliaro, M. Bearpark, J. J. Heyd, E. Brothers, K. N. Kudin, V. N. Staroverov, R. Kobayashi, J. Normand, K. Raghavachari, A. Rendell, J. C. Burant, S. S. Iyengar, J. Tomasi, M. Cossi, N. Rega, J. M. Millam, M. Klene, J. E. Knox, J. B. Cross, V. Bakken, C. Adamo, J. Jaramillo, R. Gomperts, R. E. Stratmann, O. Yazyev, A. J. Austin, R. Cammi, C. Pomelli, J. W. Ochterski, R. L. Martin, K. Morokuma, V. G. Zakrzewski, G. A. Voth, P. Salvador, J. J. Dannenberg, S. Dapprich, A. D. Daniels, Ö. Farkas, J. B. Foresman, J. V. Ortiz, J. Cioslowski and D. J. Fox, *Gaussian 09, Revision B.01*, 2009.
34 J.-D. Chai and M. Head-Gordon, *Phys. Chem. Chem. Phys.*, 2008, **10**, 6615–6620.
35 P. J. Hay and W. R. Wadt, *J. Chem. Phys.*, 1985, **82**, 299–310.
36 W. J. Hehre, R. Ditchfield and J. A. Pople, *J. Chem. Phys.*, 1972, **56**, 2257–2261.
37 R. Ditchfield, W. J. Hehre and J. A. Pople, *J. Chem. Phys.*, 1971, **54**, 724–728.
38 A. V. Marenich, C. J. Cramer and D. G. Truhlar, *J. Phys. Chem. B*, 2009, **113**, 6378–6396.
39 S. Grimme, *Chem. – Eur. J.*, 2012, **18**, 9955–9964.
40 R. F. Ribeiro, A. V. Marenich, C. J. Cramer and D. G. Truhlar, *J. Phys. Chem. B*, 2011, **115**, 14556–14562.
41 M. Álvarez-Moreno, C. de Graaf, N. López, F. Maseras, J. M. Poblet and C. Bo, *J. Chem. Inf. Model.*, 2015, **55**, 95–103.
42 R. A. Marcus, *J. Chem. Phys.*, 1956, **24**, 966–978.
43 R. A. Marcus, *Angew. Chem., Int. Ed. Engl.*, 1993, **32**, 1111–1121.
44 D. Moia, V. Vaissier, I. Lopez-Duarte, T. Torres, M. K. Nazeeruddin, B. C. O'Regan, J. Nelson and P. R. F. Barnes, *Chem. Sci.*, 2014, **5**, 281–290.
45 V. Vaissier, P. Barnes, J. Kirkpatrick and J. Nelson, *Phys. Chem. Chem. Phys.*, 2013, **15**, 4804–4814.
46 H. Huo, X. Shen, C. Wang, L. Zhang, P. Rose, L.-A. Chen, K. Harms, M. Marsch, G. Hilt and E. Meggers, *Nature*, 2014, **515**, 100–103.